Geophysical Research Letters
NOV 3 2006; 33 (21) NIL_58-NIL_63
http://dx.doi.org/10.1029/2006GL027533

An edited version of this paper was published by AGU.

High Resolution Altimetry Reveals New Characteristics of the December 2004 Indian Ocean Tsunami

Michaël Ablain[1], Joël Dorandeu[1], Pierre-Yves Le Traon[2], Anthony Sladen[3]

(1) CLS, 8-10 rue Hermes, Parc Technologique du Canal, 31526 Ramonville Saint-Agne, France
(2) IFREMER, Centre de Brest, B.P. 70 29280 Plouzané, France
(3) CEA, DASE/LDG/RSG B.P. 12 91680 Bruyères-le-châtel

Abstract:

The Indian Ocean tsunami, which occurred on December 26, 2004, was the first to be clearly observed using satellite altimeters. The wave amplitude observed in deep-ocean by TOPEX and Jason-1 was close to 60 cm about 2 hours after the earthquake. Envisat crossed the tsunami wave 3h15 after the earthquake and measured a 35 cm wave. Even though it flew over the tsunami 7h20 after the earthquake, GFO still observed a wave close to 20 cm. To better extract the tsunami signal from altimeter measurements, a specific ocean variability mapping technique is used. This technique proves to be mandatory for discriminating tsunami waves from other ocean signals. Altimeter signals are then compared with those derived from the CEA (Commissariat à l'Energie Atomique) model outputs. For the first time with altimeter data, peculiar short wavelengths signals along Jason-1 and Envisat profiles have been detected from the analysis of 20-Hz altimeter measurements. Such high wavenumber signals can be explained by the dispersive propagation of tsunami waves. These observations highlight the essential role of satellite altimeter measurements to better understand and to improve models of tsunami wave propagation and dissipation.

High Resolution Altimetry Reveals New Characteristics of the December 2004 Indian Ocean Tsunami

Michaël ABLAIN (1), Joël DORANDEU (1), Pierre-Yves LE TRAON (2), Anthony SLADEN (3)

(1) CLS, 8-10 rue Hermes, Parc Technologique du Canal, 31526 Ramonville Saint-Agne, France

(2) IFREMER, Centre de Brest, B.P. 70 29280 Plouzané, France

(3) CEA, DASE/LDG/RSG B.P. 12 91680 Bruyères-le-châtel

Abstract

The Indian Ocean tsunami, which occurred on December 26, 2004, was the first to be clearly observed using satellite altimeters. The wave amplitude observed in deep-ocean by TOPEX and Jason-1 was close to 60 cm about 2 hours after the earthquake. Envisat crossed the tsunami wave 3h15 after the earthquake and measured a 35 cm wave. Even though it flew over the tsunami 7h20 after the earthquake, GFO still observed a wave close to 20 cm. To better extract the tsunami signal from altimeter measurements, a specific ocean variability mapping technique is used. This technique proves to be mandatory for discriminating tsunami waves from other ocean signals. Altimeter signals are then compared with those derived from the CEA (Commissariat à l'Energie Atomique) model outputs. For the first time with altimeter data, peculiar short wavelengths signals along Jason-1 and Envisat profiles have been detected from the analysis of 20-Hz altimeter measurements. Such high wavenumber signals can be explained by the dispersive propagation of tsunami waves. These observations highlight the essential role

of satellite altimeter measurements to better understand and to improve models of tsunami wave propagation and dissipation.

1. Introduction

On December 26, 2004, at 0h59 p.m. UTC, an Indian Ocean earthquake with a magnitude of 9 generated a strong tsunami that produced huge waves at the coasts. The earthquake hypocenter was around 3.3°N, 95.68°E. It covered an unusually large geographical area. The East and West Bengal Gulf coasts were devastated by wave heights of up to 15 m. Propagation models show that the wave height was 60 cm in deep ocean, 2 hours after the earthquake. About 3 hours after, it dropped to around 40 cm high. After 8 hours the wave spread over most of the Indian Ocean and was between 10 and 20 cm high.

Until now, tsunami observations by satellite altimeters had not been significant. Studies carried out in the past (e.g. Okal et al.,1999) shown that only TOPEX detected a tsunami in 1992 due to an earthquake in Nicaragua. The signal has not been clearly observed because of its weak amplitude close to 8 cm and the great oceanic variability in this area. In General, the probability of detecting a tsunami by a satellite altimeter is low, because the satellite must fly over the tsunami wave with a short period after the origin time due to the great tsunami propagation speed (about 800 km/h in ocean of 5000m depth). Tsunami signals in the open ocean are also quite weak.

Because of its intensity and its large expansion, the Sumatra tsunami was detected by tidal gauges throughout the Indian Ocean (e.g. Merrifield et al, 2005). It was also the first one to be detected very clearly by TOPEX, Jason-1, Envisat and GEOSAT Follow On (GFO) satellites (e.g. Smith et al., 2005). The purpose of our paper is to concentrate on precise observations and detection by satellite. The sea level anomaly (SLA), derived

from altimeter measurements, is analyzed along the satellite passes crossing the wave front.

Observations of tsunami waves by altimetry have been already described by Gower (2006). An essential difference between this paper and the current study is the technique used to separate signals due to the tsunami from other ocean signals (e.g. large scale and mesoscale ocean variability). The technique described by Gower (2006) consists in the subtraction of the smoothed average of SLA measured on previous and next cycles over same passes. In this study, a more complex method based on a specific mapping technique is used. It allows us to better remove the oceanic signals which are not related to the tsunami. Without using this method, extraction of tsunami signals from GFO data would not have been possible. Furthermore, another originality of the current study is that high frequency signals due to tsunami waves and detected in altimeter data (Gower, 2006) have been analyzed from 20-Hz data which allows us to calculate their amplitude and their wavelength accurately. These signals could be explained by dispersive propagation.

After describing the tsunami wave for each satellite in section 3, comparisons of altimeter observations with a propagation model provided by CEA (Commissariat à l'Energie Atomique) are carried out in section 4. Section 5 describes and discusses the observation in altimeter data of peculiar high wavenumber signals explained by the dispersive propagation of tsunami waves.

2. Extraction of tsunami signals from altimeter SLA

Altimeter SLAs account for many different ocean signals such as large scale and mesoscale ocean variability. These signals modify the observed characteristics of tsunami waves and if they are of comparable amplitude, they strongly limit our ability to detect tsunami. Most of these signals can be removed, however, using an ocean anomaly

mapping technique (e.g. Le Traon et al., 1998). Note that this is possible only because we had at this time a very good space/time sampling of the ocean with four altimeters (Pascual et al., 2006).

The method consists of selecting data provided by all altimeters (Jason-1, TOPEX, GFO and Envisat) in a 40-day window centered on December, 26 2004. This day is excluded from the data window in order not to take into account measurements impacted by the tsunami. The ocean anomaly mapping technique is used to interpolate data in space and time along each altimeter profile at the tsunami day. These interpolated SLA data correspond to the sea level signals that would have been observed on December, 26, 2004, if the tsunami had not occurred. The high frequency signal is then computed as the difference between the original and the interpolated SLA. This high frequency signal is assumed to be representative of the tsunami wave, since it only reflects periods lower than about 15 days. However, other errors could remain along SLA profiles, due to corrections not perfectly taken into account in the SLA calculation such as tides or atmospheric effects.

Figure 1 illustrates the importance of applying this method in order to detect the tsunami. The full SLA measurements and the high frequency SLA are plotted along GFO pass 210. The remaining sea level anomaly observed on the high frequency SLA around latitude 45°S is associated with the tsunami, as shown in the following section. On the contrary, the prominent oceanic signal present on the initial SLA curve prevents detection of such a signal.

3. Observation of tsunami waves in altimeter measurements

Jason-1 overflew the tsunami first, 1h53 after the earthquake, on ascending pass 129 for cycle 109.The CEA model output has been mapped at this exact time on figure 2 on the

left (top) with Jason-1 pass 129 superimposed. On the right figure, the high-frequency SLA and CEA model outputs have been plotted along pass 129. The wave front of the tsunami has been observed by Jason-1 between 5°S and the equator. This first wave is divided into two peaks of nearly 60 cm amplitude. A secondary wave follows the first and is weaker, around 35 cm. The position of the wave at this time is consistent with a shallow-water wave speed of about 770 km/h which corresponds to 4500 m depth. The wave has traveled about 1500 km from the tsunami origin in the 1h53. The apparent wavelength given by the altimeter measurements is about 520 km. This figure does not take into account the time taken by the satellite to cross the wave. The satellite traveled across this wave front in about 90sec. Thus 20 km has to be added to this wavelength estimate. Finally, considering the angle between the SLA profile and the tsunami wave direction, which is about 30°, 460 km is found for the true wavelength.

TOPEX is on an orbit half-way from the Jason-1 orbit to the west and follows 7 minutes after the earthquake. Therefore, TOPEX overflew the tsunami 2h00 after the earthquake on pass 129 for cycle 452. The characteristics of the wave front are similar to these identified by Jason-1. The high-frequency SLA plotted on figure 2 (bottom) shows the main wave between 5°S and 2°S with an amplitude close to 60 cm. Notice that the wave shape is slightly different than the one observed with Jason-1, with a single wave not divided into two peaks. Data gaps due to TOPEX recorder anomalies did not allow us to analyze SLA between 1°S and 6°N. Therefore secondary waves were not detected.

The tsunami was observed by Envisat 3h19 after the earthquake on descending pass 352 for cycle 33 from the north to the south Indian Ocean between 17°S and 8°S. Despite this late observation, the signal detected by Envisat, shown on figure 3, remains very large:

about 35 cm for the first wave. As for Jason-1, a smaller secondary wave is observed between 12°S and 8°S. Its amplitude is about 25 cm.

Last observations of the Sumatra tsunami are given by GFO. The configuration of GFO passes was not optimal because the first observation occurred only 7h22 after the earthquake on descending pass 208 for cycle 143. Contrary to the other missions, the two following descending passes (210 and 212) also flew over the tsunami. They crossed the wave front at 9h03 and 10h44 respectively after the earthquake. Even with the exceptional magnitude of the Sumatra tsunami, the amplitude of the wave front becomes weak after such a period. It would be impossible to detect without removing other ocean signals. The high frequency SLA calculated from 20-Hz measurements shown on figures 5 for passes 208 and 210 shows a signal with an amplitude ranging from 15 to 20 cm between 35°S and 50°S. The CEA model outputs confirm that these signals are linked to the tsunami. The signal observed on pass 212 is not plotted due to its low amplitude, close to 10 cm according to the CEA model. The remaining oceanic signals on the high frequency SLA do not allow a clear detection of the tsunami waves. Due to the time passed after the earthquake, the GFO observations are not as clear as Jason-1, TOPEX and Envisat, but they are probably as useful to fine tune and to improve the propagation models.

4. Comparisons of altimeter observations with the CEA propagation model

The CEA model (Sladen, 2006) outputs were computed using refined initial displacement conditions derived from altimetry data. In the open ocean, the "small amplitude" approximation of the shallow water wave equations provides a linear relationship between the altimetry signal and the earthquake slip distribution. Hence, the close to the source Jason-1 track has been used to invert the contribution of 38 sub-faults, distributed

down-dip and along the 1500 km of the aftershock area. As a result, the coherence between the model and the observations has been significantly improved, compared with the first model outputs provided by CEA which did not use altimeter data. Early and recent model outputs are plotted for Jason-1 observations in figure 2. The recent CEA model outputs and the high frequency SLA show a very good agreement for the tsunami wave front for all the altimeters: amplitude and wavelength differences are weak and very well collocated in space and time. Moreover, Jason-1 SLA profile matches other significant signals which were not represented by the first CEA model outputs. Such a signal is observed between the equator and 5°N with an amplitude close to 40. These improvements demonstrate the sensitivity of the tsunami to the initial displacement conditions.

However, some signals detected in the SLA are not depicted by the model. The Jason-1 and Envisat signals seem particularly noisy close to the equator while the model is smooth. This actually corresponds to small scale oscillations which are described in the last part of this paper. Other signals, close to coasts for instance, are not well represented by the model. They could be related to the tsunami, but as this is an area of shallow waters, other errors like tidal model errors or atmospheric effects could also be present.

5. Analysis of short wavelength signals

Jason-1 and Envisat high frequency SLA profiles seem quite noisy in some places: between the equator and 3°N for Jason-1, and between 5°S and 5°N for Envisat. This apparent noise is much greater than the noise usually observed in altimeter measurements, which is about 3 cm for 1-Hz measurements (Le Traon et al., 1994). If this apparent noise is in fact a high frequency signal with a very short-wavelength, it’s not possible to analyze it accurately with the 1-Hz SLA because measurements are spaced out by about 7

km along-track and can not describe such a signal. In order to refine the SLA analyses, 20-Hz altimeter measurements available in Jason-1 and Envisat products have been used. After using the same method to remove the oceanic signals not related to the tsunami, the high-frequency SLA from 20-Hz measurements are plotted on figure 5 on the left for Jason (top) and TOPEX (bottom). For both missions, coherent oscillations are clearly visible with an amplitude between 20 cm and 25 cm. The Jason-1 wavelengths decrease from about 40 km to 30 km from south to north. For Envisat, they decrease from about 28 km to 23 km. As shown on the same figure, these oscillations are not reproduced by the CEA model. To exclude any possible explanation due to errors in altimeter measurement, all altimeter parameters and geophysical corrections used in the SLA calculation were checked. None of these are likely to explain such large oscillations.

These peculiar signals are thus probably due to the tsunami. Considering the wave propagation in dispersive medium, a simple calculation suggests that this hypothesis is conceivable. At these short wavelengths, the propagation will be dispersive and will follow the general dispersion relation for water waves (e.g. Le Blond and Mysak, 1978):

$v_{groupe} = \frac{d\omega}{dk}$ and $\omega^2 = gk\tanh(kh)$ with $k = \frac{2\pi}{\lambda}$, λ the wavelength and h the ocean depth.

Note that at long wavelengths (shallow water approximation), the relation reduces to phase velocity = group velocity phase = sqrt (gH) which is the approximation used for most tsunami models.

The tsunami group speeds are defined by the elapsed time and the distance between the tsunami origin and the satellite passes. The elapsed time is known with good accuracy, while the position of the tsunami origin does not correspond to a single point but to a rupture line over a few hundred kilometers. In a first approximation, the origin has been chosen in the center of the rupture line at 93°E, 7°N. The group speeds have been computed and plotted in figure 5 (blue curve) on the right along Jason-1 and Envisat passes. Jason-1 group speeds vary from about 540 km/h at 1°N to 490 km/h at 2°N. For Envisat, they vary from about 460 km/h at 4°S and 230 km/h at 4°N. The theoretical wavelengths are deduced from these group speeds using the dispersion relation given above. Assuming a uniform depth of 4500 m, in the Jason-1 case, the theoretical wavelengths associated to the previous group speeds vary from 32 km at 1°N to 27 km at 2°N. For Envisat, they vary from 24 km at 4°S to 10 km at 4°N. They must be divided by the cosine angle between the satellite pass and the wave propagation, in order to be compared with the apparent wavelengths in altimeter measurements. Then, the apparent theoretical wavelengths are plotted on same figure 5 (red curve) on the right along Jason-1 and Envisat passes. They vary from 37 km at 1°N to 32 km at 2°N for Jason-1 and from 27km at 4°S to 17km at 4°N. They are thus very similar to the observed wavelengths described previously with differences smaller than 3 km. This is a remarkable agreement between theory and observations.

6. Conclusion

For the first time, tsunami waves in the open ocean have been clearly measured by satellite altimetry. This is due to the exceptional intensity of the Sumatra tsunami but also to a unique configuration of four altimeters flying simultaneously. Such a configuration is necessary to describe and forecast the ocean mesoscale variability (e.g. GODAE, 2001;

Pascual et al., 2006). It allowed us to extract the signals due to the tsunami from the background ocean variability signals. The mapping method used in this study allowed to remove realistic ocean signals not related to the tsunami. The tsunami signal has been extracted from all altimeter missions flying at that time and has been observed with good accuracy, as demonstrated by the consistent comparisons with the CEA model.

However, the barotropic model could not reflect short wavelength signals yet well observed by high frequency altimetry. These realistic signals prove to be due to the tsunami since they are consistent with propagation theory in a dispersive medium.

Satellite altimetry is, however, inadequate for early detection and warning. Even with a four altimeter configuration, the probability of observing a tsunami just after it was triggered remains low (e.g. Okal et al., 1999). This also poses some specific data acquisition and processing issues. This does not mean, however, that one should not take advantage of high resolution altimeter systems to complement operational warning systems.

However, this study demonstrates that the main and unique contribution of satellite altimetry is to better understand and to improve the modeling of tsunami propagation and dissipation. Observations reported here have been used, in particular, to refine the initial displacement conditions due to the earthquake so that observations match model outputs.

Acknowledgements

This work was supported by CNES (Centre National d'Etudes Spatiales). The altimeter products have been produced by SSALTO/DUACS and are distributed by AVISO. Thanks to E. Okal for his precious comments about the oscillations on 20-Hz measurements.

Reference

Le Blond, D. H., and L. A. Mysak, 1978: Waves in the Ocean. Elsevier, 602 pp.

Le Traon, P.Y., F. Nadal, and N. Ducet, 1998. An improved mapping method of multi-satellite altimeter data. J. of Atmos. & Oceanic Tech., 15, 522-534.

Le Traon, P.Y, Stum, J. Dorandeau, and P. Gaspar, 1994, Global Statistical Analysis of TOPEX and POSEIDON Data, Journal of Geophysical Research, 99(C12).

Merrifield, M. A., et al., 2005, Tide gauge observations of the Indian Ocean tsunami, December 26, 2004, Geophys. Res. Lett., Vol. 32, No 9.

Okal, E., Piatanesi, A. and Heinrich, P. 1999. Tsunami detection by satellite altimetry. Journal of Geophysical Research 104 (B1).

Pascual, A., Y. Faugère, G. Larnicol, P.Y. Le Traon, 2006, Improved description of the ocean mesoscale variability by combining four satellite altimeters. Geophys. Res. Lett., Vol. 33, No. 2.

Smith, W. H. F., R. Scharroo, V. V. Titov, D. Arcas, and B. K. Arbic, 2005: Satellite altimeters measure tsunami. Oceanography, 18(2), 11-13.

Gower, J, The 26 December 2004 tsunami measured by satellite altimetry, 2006, IJRS, submitted

The International GODAE Steering Team, 2001: The Global Ocean Data Assimilation Experiment Strategic Plan. GODAE report n°6 Australia, Melbourne.

Sladen A., Hebert H., On the use of satellite altimetry to infer the rupture history of the 2004 Sumatra earthquake, 2006, GRL, submitted

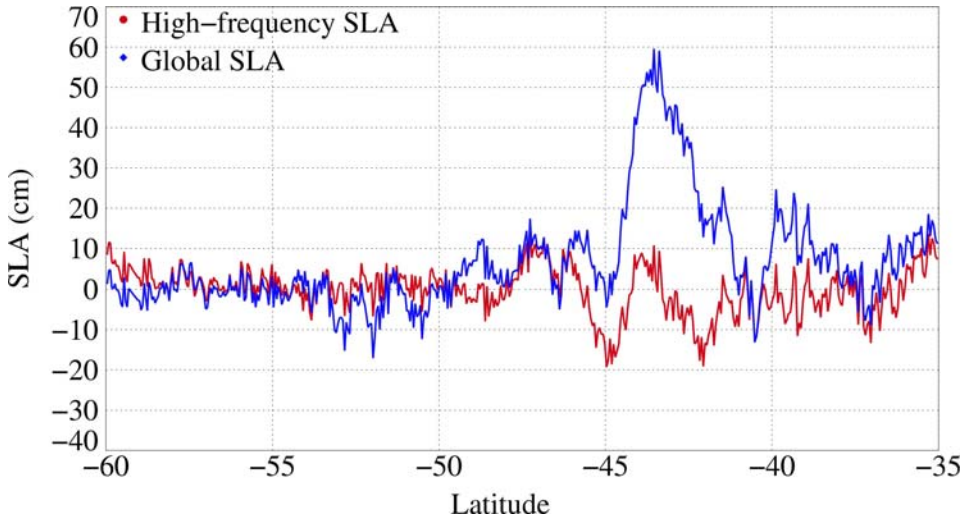

Figure 1 : Initial SLA and high-frequency SLA on GFO pass 210. High-frequency SLA highlights the weak tsunami signal observed around 45°S while this signal is totally hidden by other oceanic signals in the initial SLA curve.

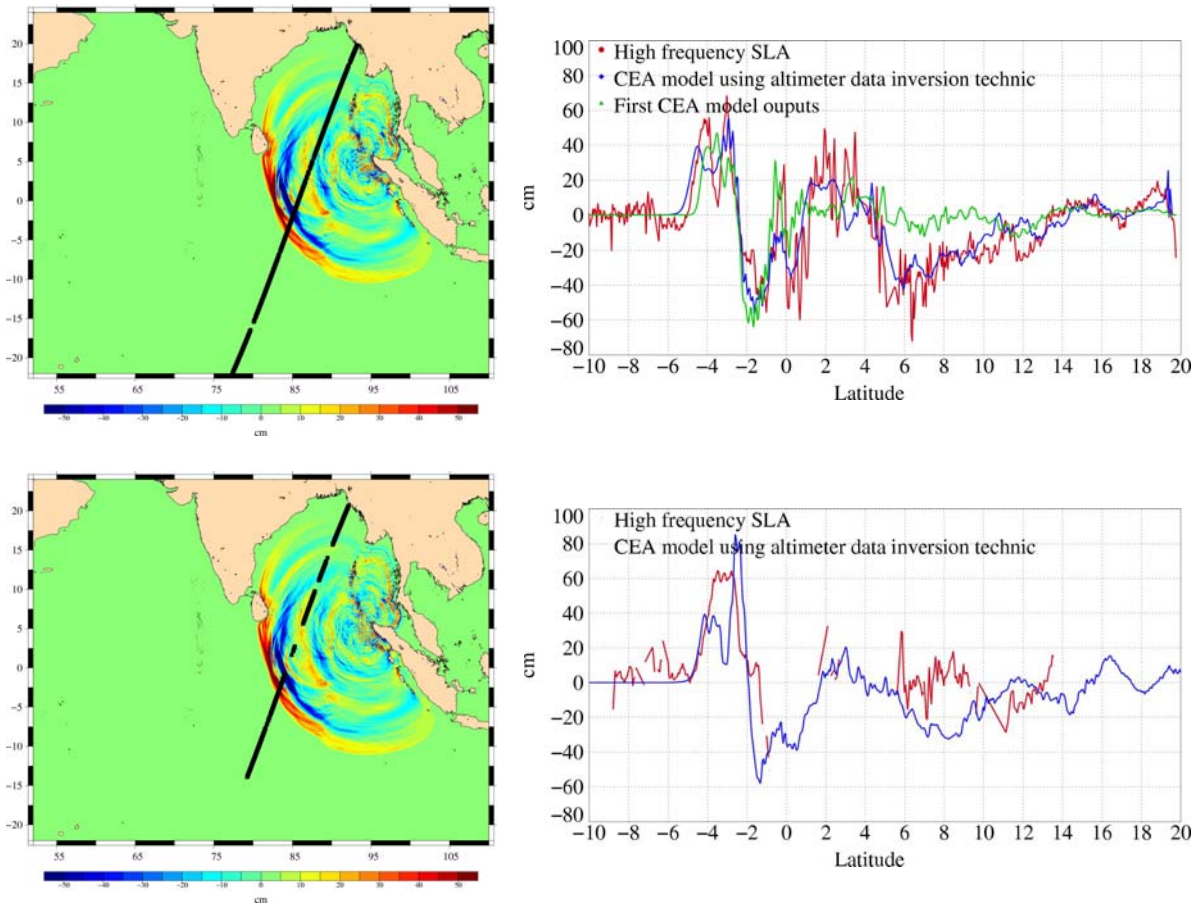

Figure 2 : Left: tsunami wave heights, as computed by the CEA model, 1:53 hour (top) and 2:00 (bottom) after the earthquake with respectively Jason-1 and TOPEX pass 129 superimposed. Right: high-frequency SLA, and CEA model outputs along Jason-1 (top) and TOPEX (bottom) pass 129. For Jason-1, the first and new CEA model outputs have been plotted.

275

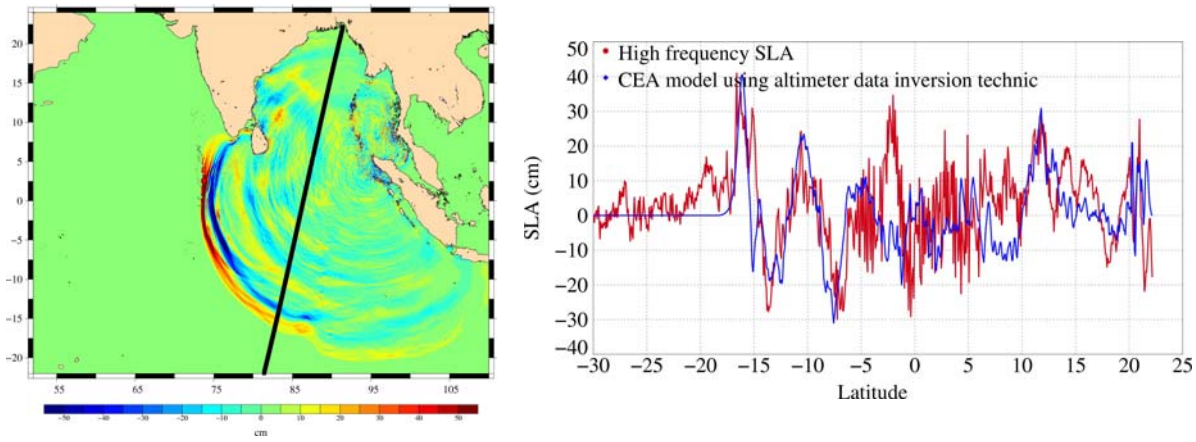

Figure 3 : Left: tsunami wave heights, as computed by the CEA model, 3:15 hours after the earthquake. Envisat pass 352 is superimposed. Right: High-frequency SLA, new and first CEA model outputs along Envisat pass 352.

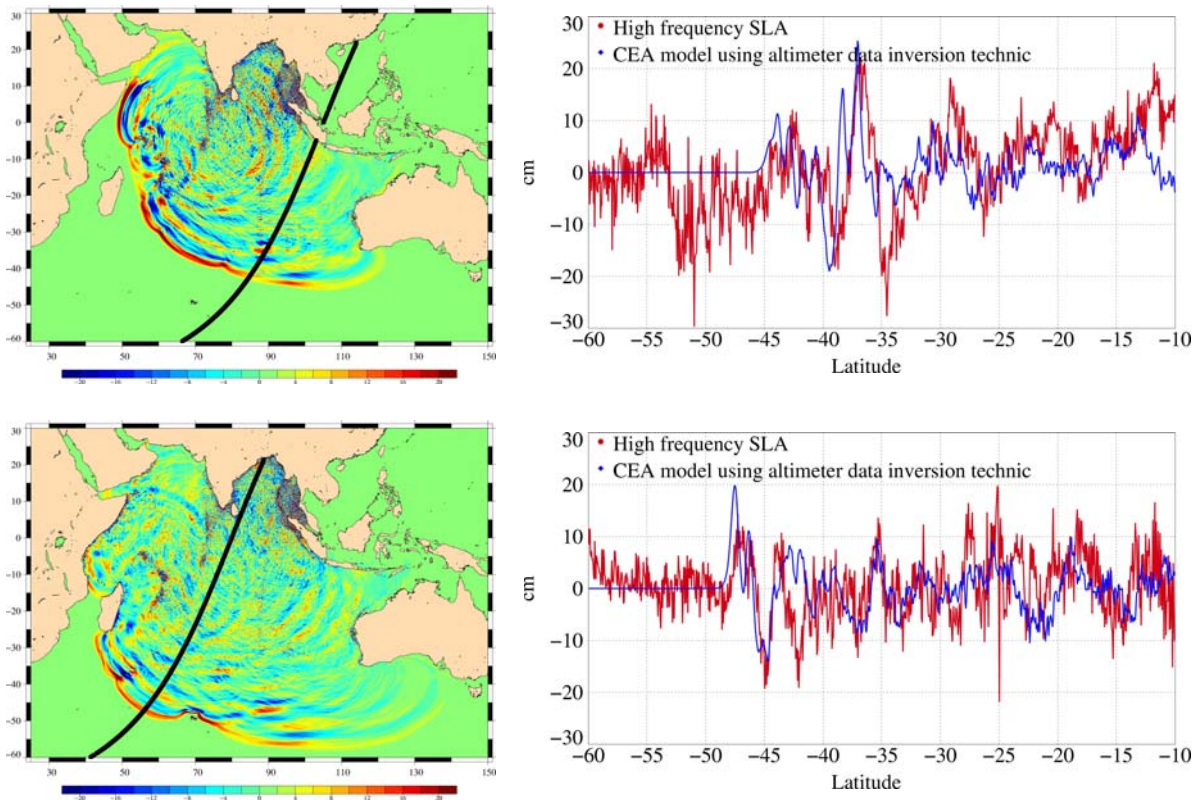

Figure 4 : Left: tsunami wave heights as computed by the CEA model, 7:00 hours (top) and 9:00 (bottom) hours after the earthquake with respectively the GFO pass 208 and 210 superimposed. Right: high-frequency SLA and CEA model output along GFO pass 208 (top) and 210 (bottom).

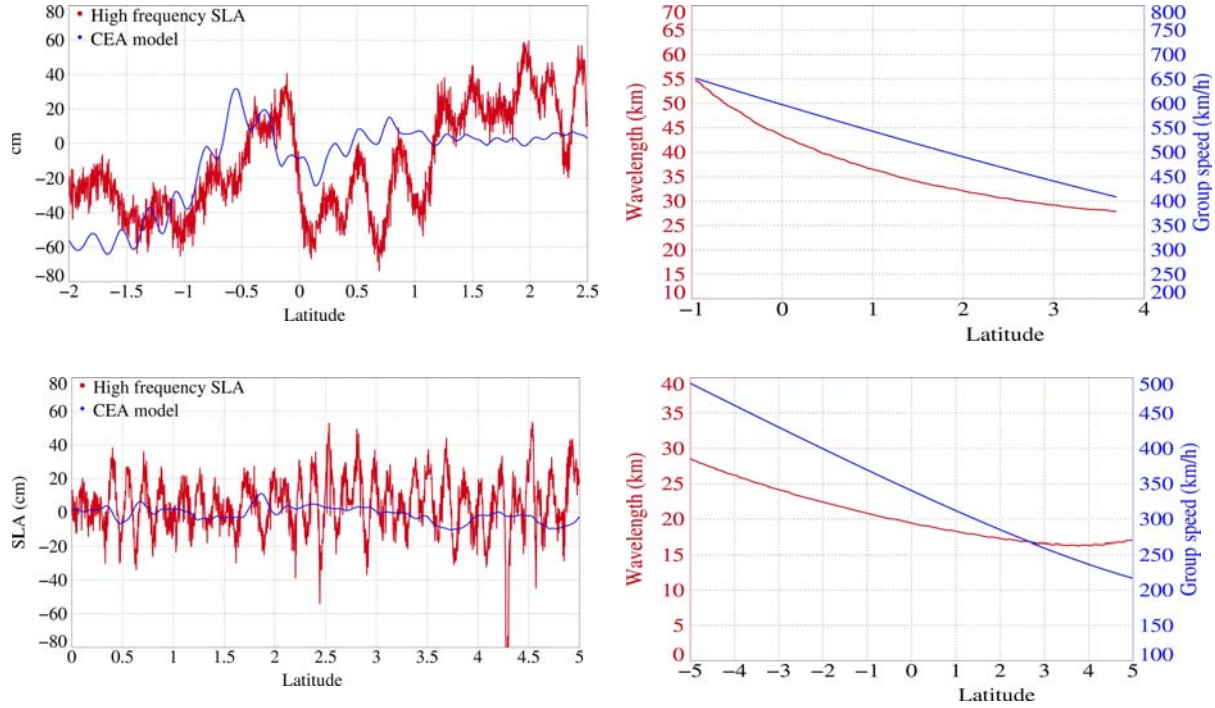

285 **Figure 5 : Left : CEA model outputs and high frequency SLA from 20-Hz measurements for Jason-1 (top) and Envisat on (bottm). Right: Group speeds (blue curve) and apparent theoretical wavelengths (red curve) for Jason-1 (top) and Envisat (bottom). The apparent theoretical wavelengths correspond to the theoretical wavelengths divided by the angle cosine between the satellite pass and the wave propagation.**

290